

Uncertainty in Flow in Porous Media

Problem presented by

Daniel Busby and Chris Farmer
Schlumberger Abingdon Technology Centre

Problem statement

The problem posed was, in essence, how do we estimate the probability distribution of $f(x)$ from the probability distribution of x ? Here x is a large vector and f is a complex function which can be expensive to evaluate. For Schlumberger's applications f is a computer simulator of a hydrocarbon reservoir, and x is a description of the geology of the reservoir, which is uncertain.

Study Group contributors

Joyce Aitchison (JMA Numerics)
Kseniya Arsentieva (University of Oxford)
Linda Cummings (University of Nottingham)
Jason McVean (??)
Dhanesh Patel (??)
Giles Richardson (University of Nottingham)
Jonathan Rougier (University of Durham)

Report prepared by

Joyce Aitchison (JMA Numerics)
Linda Cummings (University of Nottingham)
Giles Richardson (University of Nottingham)
Jonathan Rougier (University of Durham)

1 Introduction

The problem posed was, in essence, how do we estimate the probability distribution of $f(x)$ from the probability distribution of x ? Here x is a large vector and f is a complex function which can be expensive to evaluate. For Schlumberger's applications f is a computer simulator of a hydrocarbon reservoir, and x is a description of the geology of the reservoir, which is uncertain. We might also want to update our distribution on $f(x)$ to include information relevant to some of the simulator output values. Typically this would be production history for a reservoir that had been operational for some time, and for which the simulator was being run forwards into the future to evaluate a possible control regime.

We broke this problem into three parts. The first is reducing the dimensionality of the input space, discussed in section 2. The second is performing the inferential calculations despite only having a limited number of simulator evaluations. The calculations are discussed in section 4, while the technology necessary to make these calculations feasible, namely an emulator, is discussed in section 3. The final part is having available a number of test problems for which we could compute exact solutions, for evaluative purposes. Two different approaches are presented in sections 5 and 6, relating to flow in a porous medium in the presence of narrow faults or cracks. These final two sections can be read independently of the previous ones.

2 Dimensional Reduction

2.1 Grid-independent representation of fields

Many of the uncertain inputs to a reservoir simulator are fields. These include the scalar porosity field and the permeability tensor, which are both 3D, and the aquifer pressure and fault transmissibilities, which may be taken as 2D manifolds. Notionally these fields are infinite-dimensional. However, because they are smooth we can hope to represent them with acceptable fidelity using a finite number of quantities.

For inferential purposes we must restrict the number of quantities to, say, a few hundred at most. This figure is likely to rise slowly as computing power increases, but it is and will remain several orders of magnitude short of the number of grid cells in a modern simulator. This means that current representations as values specified for each grid cell are not tenable. This does not mean that we do not compute and use a value for each grid cell at the point where we evaluate the simulator, but rather that these values must be derived from from an underlying representation that is smoother.

Perhaps the strongest conclusion from the workshop is that we must find ways to represent these fields in a grid-independent way. This involves two related challenges. First, we must represent the field as an uncertain quantity, in a manner that allows the experts to 'tune' the behaviour of the realisations of the field according to their knowledge, and to information from sources such as seismic studies and well-logs. We must also attempt to

make this representation sensitive to the information contained in the production history, for history-matching. In other words, if the production data want to tell us about the mean permeability of the reservoir, then mean permeability should be a feature of our representation. For this reason it seems natural to want to represent the features of each field as an ordered collection of quantities going from highly aggregated to highly localised. This is discussed in section 2.2.

The second challenge is to find a way to go from the field representation to the appropriate value for any given grid cell, known generically as the problem of upscaling. For porosity this is straightforward, since a simple average (integration of the field over the cell) would seem to be appropriate. The problem for permeability is known to be far less tractable. In the workshop we discussed the problem of permeability upscaling and proposed an approach based on physical insight, discussed in section 2.3.

2.2 Random field representations

For simplicity consider a real-valued scalar random field f defined on a vector-space with representative element x . If we are uncertain about this field then we may describe our uncertainty in terms of a mean function μ and a variance function κ , where

$$\mu(x) := \mathbf{E} (f(x) | x) \tag{1}$$

$$\kappa(x, x') := \mathbf{Cov} (f(x), f(x') | x, x'). \tag{2}$$

The basic theory of random fields is given in Bartlett (1978). In the Bayesian interpretation of Kriging, a random field with given mean function and variance function describes the prior distribution, which is then updated using observations. Details may be found in Handcock and Stein (1993), and the references in Kennedy and O’Hagan (2001). If the prior is taken to be gaussian then the conditional field is also gaussian; more generally, the updated mean function is the best predictor of the field under the principle of minimised quadratic loss. This is an example of the *Bayes linear* approach, outlined in Goldstein (1999). This approach will be discussed below, in section 3.3.

As is typical in Bayesian applications, where there is lots of observational data the precise choices for μ and κ do not matter very much, and it is not unreasonable to treat the prior field as second-order stationary, *i.e.* with a constant mean function and a variance function with a simple parameterisation that depends only on the vector $x - x'$. One choice, which is appropriate for fields that are believed to have sample paths that are infinitely differentiable (in the mean-squared sense), is

$$\kappa(x, x') = \sigma^2 \exp \left\{ -\theta \|x - x'\|^2 \right\} \tag{3}$$

where $\|\cdot\|$ is the euclidean norm. With this choice it is necessary to specify the variance σ^2 and the ‘decay rate’ θ . The reciprocal of this decay rate controls what might be termed the field’s correlation length (large decay rate implies short correlation length).

Where there is not much data, it is important to be able to incorporate much more detailed prior knowledge, *i.e.* to make a quite precise statement about μ and κ . Often it

is hard to do this directly, particularly while ensuring that κ remains positive definite. One method discussed at the workshop was to start with a quite general mean and variance (*e.g.*, the stationary form given above) and then to introduce *pseudo data* with which to condition the field. To give a simple example, suppose that the value of the field was thought to be close to 1 at location x . We could introduce a pseudo datum taken at x with value 1. If we treated that datum as certain then by conditioning the field we would force all of its realisations to pass through 1 at x ; if we treated the pseudo datum as noisy, say with standard deviation 0.1, then we could arrange for most of its realisations to pass within 0.3 of 1 at x . By introducing a few of these pseudo data it is possible to create quite a general structure in realisations of the random field. The actual impact of each datum depends on the decay rate, and the presence of other data, both pseudo and real. In the workshop we discussed presenting a sequence of realisations of the field to the engineer with a visualisation tool, which would allow tuning of the values and locations of the pseudo data to achieve the desired effect. It is important to remember that some of the pseudo data could actually be located outside the reservoir.

We have not yet discussed the main advantage of a random field representation. This type of representation lends itself naturally to a finite-dimensional reparameterisation. We can choose a complete basis for the vector-space containing x , and then project the field onto the basis. So, for example, we can write

$$f(x) = \sum_{j=0}^{\infty} \beta_j L_j(x) \quad (4)$$

where $B = \{\beta_j\}$ are the fourier coefficients for the orthonormal basis $L = \{L_j\}$. As L is known, all of the randomness of f is now contained in the joint distribution of B . We can expect the contribution of the β_j terms to the variation of f to vary according to the order of L_j , and it follows that by a careful choice of basis we can get reasonably close to representing f with only a moderate number of terms.

We compute the mean and variance of B using the underlying mean function and variance function of f . For example, consider computing the mean of β_j :

$$\mathbf{E}(\beta_j) = \mathbf{E}(\langle f, L_j \rangle) = \langle \mathbf{E}(f), L_j \rangle = \langle \mu, L_j \rangle \quad (5)$$

where $\langle f, f' \rangle := \int f(x) f'(x) dx$. A similar calculation using the variance function gives the variances and covariances of B . A natural approach to deciding on a finite representation for f is to compute the variances for lots of the coefficients in the basis, and then keep as many as is necessary to have, say, 95% of the variation of the field when averaged across the possible values for x . The variance contribution of the truncated terms should be added back in, by appending a nugget term.

The choice of basis is up to the engineer, but a natural choice in the first instance is a polynomial basis, namely the legendre polynomials shifted onto an appropriate interval. Sticking, for simplicity, with a single dimension for x , L_0 is a constant and so β_0 picks up the mean field value. Then β_1 picks up the difference between left- and right-hand field values, β_2 the difference between middle and edge values, and so on. The B coefficients become the grid-free representation of the field. A realisation of the field is created by

generating a realisation of the B coefficients, probably using a gaussian or a multivariate t distribution. Learning about the field, *e.g.* by calibration, is learning about the B coefficients. In this way it is possible, by our choice of L , to direct the calibration data towards those aspects of the field that are thought by the engineer to be most relevant to the data itself, *e.g.* the mean field value (β_0 in the legendre basis).

2.3 A grid-free permeability model

We spent a session brain-storming the problem of permeability upscaling, and the implications that this might have for a grid-free representation of the permeability tensor. We thought we might reduce the permeability field to a network of channels extending through the reservoir. Then the upscaling problem for a given cell block consists of counting pathways that enter the cell at one given face, and leave at another. We thought we might be able to represent beliefs about permeability in terms of beliefs about the parameters of a random network defined on vertices that filled, in some fashion, the reservoir. This network need not be a simple lattice: in general it would be described by a collection of vertices at specified locations with a given neighbourhood structure.

Typically the parameters of a random network describe the probability of finding a link between two neighbouring vertices depending on the other links in the localised region. In this way we can control the density of the pathways, and the distribution of their lengths. These macro-scale features would seem to be strongly related to permeability, as described above. Thus if the parameters themselves are described as a field over the reservoir, then this would allow us to describe how permeability varied over the reservoir. This parameter field could be quite smooth and low-dimensional, allowing us to represent the permeability tensor in a finite and hopefully small collection of values, perhaps using the projection method outlined above.

We discussed an experiment to see whether this approach would be useful. We could take a collection of vertices in a 3-D space, and within that space identify a grid cell. For a given set of random network parameters we could generate a number of realisations of a permeability network. For each realisation we could compute the effective cell permeability by treating the network as narrow channels through an impermeable medium. We could then study how the mean and variance of the effective permeability varied as we varied the random network parameters, and as we varied the grid cell size. This would seem to be a natural experiment for a PhD student.

3 Introducing an Emulator

In this section and in section 4 we treat the dimensional-reduction problem as solved. In other words, the engineers' uncertainty about the inputs to the simulator has been reduced to a probability distribution over a vector of moderate length.

3.1 The role of the emulator

An emulator is a statistical model for the simulator. The key point to grasp is that it is more than a simple interpolator. For any finite collection of simulator inputs the emulator describes the joint probability distribution of the resulting outputs. In the simplest case, for any given input value the emulator tells us what the simulator might say were it to be evaluated at that input, in terms of a mean and variance. Typically a simulator has many outputs, so this is in fact a mean vector and a variance matrix. We would often take our emulator to be a gaussian random field over the input space, possibly after transformations, in which case the simulator output at any given input is a gaussian random vector.

The key role of the emulator is to replace the simulator in inferential calculations. We are going to want to sample the input space, and without an emulator we would have to evaluate the simulator for every point we sample. With the emulator we can replace the evaluation of the simulator at a known input with a sample from the emulator at that input. This sample only takes a moment, and so we can get literally millions of samples from our emulator in the time it takes to evaluate the simulator once. The importance of this is discussed in section 4.

3.2 Building an emulator

An emulator is another example of a random field, and therefore we retain the previous notation. Now the simulator is f , and the vector of simulator inputs is x . By and large we expect emulators to have a much more complicated structure than simple physical random fields, and methods for emulator construction are under active development in the statistical community: Kennedy and O’Hagan (2001) and Craig et al. (2001) give two alternative methods. The former is relatively close to Kriging with vague prior information, while the latter, designed explicitly for cases like reservoir modelling in which the simulator is very expensive to evaluate, tends to make greater demands on the expert and on alternative sources of information about the simulator.

The Craig et al. approach is to construct an emulator of the form

$$f_i(x) = \sum_{j \in J_i} \beta_{ij} L_j^{(i)}(x_{(i)}^*) + \epsilon_i(x) \quad i = 1, \dots, k. \quad (6)$$

Here $x_{(i)}^*$ is a collection of *active* variables for each output, being the variables to which f_i is most responsive. The basis functions are selected individually for each output, and the residual term $\epsilon_i(x)$ typically contains a smooth random field in $x_{(i)}^*$ and a nugget for excluded variation in $x \setminus x_{(i)}^*$. It is natural to set the decay rate of the random field to account for the lowest-order term excluded from the basis. Thus if the basis comprises linear, quadratic and two-way interaction terms then the decay rate is chosen to give realisations that look at least cubic. The dominant part of this emulator is the collection of uncertain coefficients $B = \{\beta_{ij}\}$.

An interesting empirical observation is that although the time-path of simulator outputs can be complicated, the response of that time-path to variations in the simulator inputs

is often quite simple. Suppose that $f(x)$ represents an output at a well measured through time. In this case $f_i(x)$ is the observation at one particular time. Now the collection $(f_1(x), f_2(x), \dots, f_k(x))$ is a time series that can show complex temporal behaviour (in terms of simple basis functions like polynomials); for example it might be exponential or sigmoidal. But the response of that collection to changes in x is quite simple. Typical patterns would be a vertical shift in the whole curve, or a tilt, or a bend. What this means in practice is that the sets J_i tend to be quite small, while still explaining a large amount of the variation in f_i to changes in x . So a simulator may be quite a complicated function, but if a lot of that complexity happens in the time-domain it is still possible to build cheap and effective emulators.

There are several ways to build emulators such as (6). Where the simulator is not too expensive to evaluate, we may start with a collection of *scoping runs*: enough for us to do some intensive data analysis to pick out good choices for the basis functions and to estimate the mean and variance of B . Another possibility is to build a coarse version of the simulator to do the scoping runs. A third is to squeeze as much information as possible from the evaluations of the simulator by having it output derivatives. For example a few evaluations including derivative information may be enough to identify the active variables for each output. Automatic code differentiators may be helpful here.

Our choices for the emulator are not set in stone, and may be modified, within reason, in response to diagnostic information. Diagnostics are crucial, and are discussed at the end of section 3.3.

3.3 Updating the emulator

The emulator allows us to compute the mean vector and covariance matrix of the outputs for any given finite collection of inputs. Suppose we have evaluated the simulator n times, at inputs $X = (x_1, \dots, x_n)$, so that we have a vector of outputs $F = (f(x_1), \dots, f(x_n))$. If we want to compute the mean and variance of the simulator at another input $x \notin X$ we can do it using the updating formulae

$$\mathbf{E}(f(x) | F) = \mathbf{E}(f(x)) + \text{Cov}(f(x), F) \text{Var}(F)^{-1} (F - \mathbf{E}(F)) \quad (7)$$

$$\text{Var}(f(x) | F) = \text{Var}(f(x)) - \text{Cov}(f(x), F) \text{Var}(F)^{-1} \text{Cov}(F, f(x)) \quad (8)$$

where x and X are given throughout. If we assume that f is a gaussian random field then these are the conditional mean and variance of a gaussian distribution. But there is a more general justification under the Bayes linear approach, and we would refer to these as the adjusted mean and variance, with no further distributional specification. Obviously the expensive part of this calculation is the inversion of the variance matrix, which is of size $kn \times kn$, but this only has to be done once per evaluation. Also, it can be done sequentially per evaluation by partitioning, although this method is suspected of introducing numerical instability.

In the case where $x \in X$, say $x = x_n$, it is easy to verify that $\mathbf{E}(f(x)) = f(x_n)$ and $\text{Var}(f(x)) = \mathbf{0}$. This just states that the emulator interpolates the evaluations of the simulator, as you might expect. It is often observed that the behaviour of the emulator

inside the convex hull of X is usually fairly robust to the precise specification of B and ϵ , particularly when f is thought to be quite smooth. What is less often appreciated, however, is that the proportion of the input space occupied by the convex hull declines dramatically with the size of the input space: typically $f(x)$ is an extrapolation. This suggests that great care should be taken when constructing the emulator, and that diagnostics should be computed.

The easiest and most intuitive diagnostic is the one-step-ahead prediction. Each time we evaluate the simulator, we use the emulator to predict the outcome. Then we compare the actual outcome with its predicted mean and variance. Single-value statistics like the Mahalanobis distance are useful, but usually a more detailed examination is called for, to see whether alarming mis-predictions can be attributed to an input, or can be localised in space or in time. Although technically double-counting the data, a certain amount of intervention to correct the behaviour of the emulator is not unreasonable. This will usually take the form of increasing (or, occasionally, decreasing) the variances of some of the B coefficients.

4 Inference

There are two types of inferential calculation we might want to perform: *uncertainty analysis* and *calibrated prediction*. Uncertainty analysis is learning about how uncertainty in the simulator inputs feeds through into uncertainty in the simulator outputs. In other words, given a probability distribution $\Pr(x^*)$, what is the distribution of $f(x^*)$? Calibrated prediction introduces data on some of the simulator outputs, say z . The problem is: given $\Pr(x^*)$ and z , what is the joint distribution of $(x^*, f(x^*))$? In both of these problems x^* is the correct simulator input, the value of which is uncertain. Note that statisticians active in the area of simulator-based inference reject outright the notion that there can be a correct input for an imperfect simulator, but the generalisation, discussed for example in Craig et al. (2001) and Goldstein and Rougier (2004), is in principle straightforward, and so will not be considered here. Uncertainty analysis is in fact a part of calibrated prediction, and so the two will be discussed together.

4.1 Calibrated prediction

Our objective is to describe the joint distribution of $(x^*, f(x^*))$, either unconditionally (uncertainty analysis), or conditionally on z (calibrated prediction). In both cases we will also condition on the set of n simulator evaluations, namely F . The precise method we use, for there are many, will depend on how large the problem is, how the simulator is expected to behave, and what kind of information is required from the analysis. For example, we can summarise the target distribution in terms of a random sample, or in terms of an estimate of the mean, variance, and other characteristics. A simple introduction to sampling-based inference is given in Smith and Gelfand (1992), while details of the various methods are available in Ripley (1987), Robert and Casella (1999) or Evans and Swartz (2000).

For illustration, consider the case where we want to find the mean of x^* conditional on the simulator evaluations F and the data z . This is the probabilistic equivalent of history matching. We must describe the measurement errors in z in terms of a *likelihood function*

$$L_z(y) := \Pr(z | y) \quad (9)$$

where $y := f(x^*)$ is the true reservoir value. Often this likelihood function is quite straightforward; *e.g.*, in the case where each observation is subject to an independent gaussian measurement error with zero mean and known variance. A natural estimator of the mean is then

$$\hat{Q}_m := \sum_{j=1}^m w_j x_j \quad \text{for which} \quad \begin{cases} x_j \stackrel{\text{iid}}{\sim} \Pr(x^*) \\ y_j \stackrel{\text{iid}}{\sim} \Pr(f(x_j) | F) \end{cases} \quad (10)$$

where $w_j \propto L_z(y_j)$ and $\sum_{j=1}^m w_j = 1$. In words, we sample a value x_j from $\Pr(x^*)$, then we sample an output from the emulator at input value x_j , namely y_j . This value of y_j determines the weight in the weighted mean calculation, so that y_j values that better match the data z get a larger weight.

The estimator \hat{Q}_m has the property that $\lim_{m \rightarrow \infty} \hat{Q}_m = \mathbf{E}(x^* | z, F)$, by the Strong Law of Large Numbers. Hence the importance of replacing the simulator with an emulator: we need to be able to make m large in order to have confidence in the result, and this is not possible if we only have the simulator, and that simulator takes anything greater than a few seconds to evaluate.

If we wanted the mean value for $f(x^*)$, where the simulator f might be run forwards into the future, for example to evaluate a location for a new well, then we would simply replace x_j in \hat{Q}_m with y_j . We could also generalise \hat{Q}_m in the obvious way to compute the variance of $(x^*, f(x^*))$, or higher moments such as the skewness and kurtosis. Alternatively we could estimate probabilities by replacing x_j by the indicator function of any given event, *e.g.* using $I(y_{jv} > 10)$ would estimate the probability that output v of the simulator was greater than 10.

If we wanted to do simple uncertainty analysis, *i.e.* if we do not have any data so $z = \emptyset$, then we replace w_j by $1/m$. Obviously the conditional mean of x^* in this case is the same as the mean of $\Pr(x^*)$, but by replacing x_j with y_j we can compute the mean of $f(x^*)$, and its higher moments, based on our n evaluations F . Therefore in the fully probabilistic approach the difference between uncertainty analysis and calibrated prediction comes down simply to modifying the weighted sum according to the likelihood.

Note that Craig et al. (1996, 1997, 1998) have suggested an alternative approach to calibration, which is more straightforward to implement. Its principle is to rule out regions of the input space according to z , using a measure they term ‘implausibility’. It still uses an emulator, but typically the emulator can be simpler, because it is not necessary when using the implausibility measure to represent the full multivariate structure of the simulator output. This approach has been adopted in a commercial software tool, EnABLE, available from Energy SciTech Ltd. (<http://www.enscitech.com>).

4.2 Optimal design

When the simulator is expensive to evaluate, we want to pick each input at which we evaluate with care. Note that where we have an emulator we do not have to pick the simulator evaluation points according to $\Pr(x^*)$; rather we have to sample x^* according to $\Pr(x^*)$ and then sample the emulator at each value. This leaves it open for us to choose each evaluation of the simulator according to some kind of optimality criterion. The most natural one is to look at the reduction in predictive variance for various possible choices for x_{n+1} . For each candidate value x for x_{n+1} we pretend we have evaluated the simulator at x , and we use the emulator mean to generate a synthetic output value. Then we perform the inferential calculations as though we had $n + 1$ evaluations rather than n , for example those outlined in section 4.1, and score x according to its ability to reduce the variance of inputs or outputs about which we are particularly interested. Obviously we cannot expect to find the best candidate for x_{n+1} in this way, but we can at least avoid making a bad choice.

This approach to sequential design operates one step ahead. If the simulator is currently evaluating x_{n+1} then we can be computing a good value for x_{n+2} offline by using the emulator to synthesise values for both $f(x_{n+1})$ and $f(x)$ where x is our candidate value for x_{n+2} . If we know we have a fixed number of evaluations left to do then we can go further. Suppose we have 4 evaluations left in our budget. We can simultaneously choose (x, x', x'', x''') as candidate values for x_{n+1}, \dots, x_{n+4} . Then, once we are evaluating our chosen x_{n+1} , we can re-choose x_{n+2}, \dots, x_{n+4} , and so on. Obviously this approach is more powerful than one-step-ahead because it builds into our choice of the next evaluation the knowledge of the total number of evaluations available.

5 Darcy flow in an oil reservoir

In this section we explore some computable examples of fluid flow in a porous medium, subject to constraints.

5.1 Darcy flow around a thin region of different permeability

Consider fluid within a porous medium, flowing in two dimensions under Darcy's law around the thin slit like geometry (with aspect ratio ε) between the curves $y = \varepsilon f^+(x)$ and $y = \varepsilon f^-(x)$ for $|x| < a$ (shown in figure 1). Here

$$\nabla \cdot (k \nabla p) = 0 \quad \text{in } \mathbb{R}, \quad \text{where } k = \begin{cases} k_1 & \text{in } \Omega^c \\ k_2 & \text{in } \Omega. \end{cases}$$

Writing $p = p_1$ in Ω^c and $p = p_2$ in Ω gives the equivalent problem

$$\nabla^2 p_1 = 0 \quad \text{in } \Omega^c \tag{11}$$

$$\nabla^2 p_2 = 0 \quad \text{in } \Omega \tag{12}$$

$$p_1 = p_2 \quad \text{and} \quad k_1 \frac{\partial p_1}{\partial n} = k_2 \frac{\partial p_2}{\partial n} \quad \text{on } \partial\Omega. \tag{13}$$

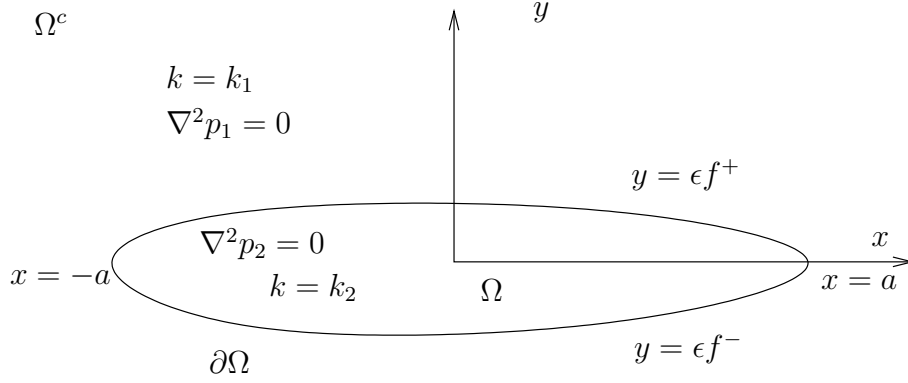


Figure 1: Geometry of the flow considered in section 5.1

There turn out to be two cases of particular interest: when the ratio of the permeabilities $\lambda = k_1/k_2$ is (i) large, $\lambda \gg 1$ and (ii) small, $\lambda \ll 1$. Before considering these cases in detail we rescale y (in Ω) with ε , so that $y = \varepsilon Y$, and rewrite equations (11)–(13) in the form

$$\nabla^2 p_1 = 0 \quad \text{in } \Omega^c \quad (14)$$

$$\frac{\partial p_2}{\partial Y^2} + \varepsilon^2 \frac{\partial^2 p_2}{\partial x^2} = 0 \quad \text{for } f^-(x) < y < f^+(x), \quad |x| < a \quad (15)$$

with

$$\left. \begin{aligned} p_1 &= p_2 \\ \lambda \left(\frac{\partial p_1}{\partial y} - \varepsilon f^{+'} \frac{\partial p_1}{\partial x} \right) &= \left(\frac{1}{\varepsilon} \frac{\partial p_2}{\partial Y} - \varepsilon f^{+'} \frac{\partial p_2}{\partial x} \right) \end{aligned} \right\} \text{on } y = \varepsilon f^+(x), |x| < a \quad (16)$$

and

$$\left. \begin{aligned} p_1 &= p_2 \\ \lambda \left(\frac{\partial p_1}{\partial y} - \varepsilon f^{-'} \frac{\partial p_1}{\partial x} \right) &= \left(\frac{1}{\varepsilon} \frac{\partial p_2}{\partial Y} - \varepsilon f^{-'} \frac{\partial p_2}{\partial x} \right) \end{aligned} \right\} \text{on } y = \varepsilon f^-(x), |x| < a. \quad (17)$$

Case (i) $\lambda \gg 1$

In this instance the canonical scaling is $\lambda = 1/\varepsilon$ (the behaviour in the cases $1 \ll \lambda \ll 1/\varepsilon$ and $\lambda \gg 1/\varepsilon$ can be deduced from the canonical case). The expansions for p_1 and p_2 proceed as follows:

$$p_1 = p_1^{(0)} + \dots \quad \text{and} \quad p_2 = p_2^{(0)} + \dots$$

The leading order problem for p_2 is thus

$$\frac{\partial^2 p_2^{(0)}}{\partial Y^2} = 0, \quad (18)$$

$$\left. \frac{\partial p_2^{(0)}}{\partial Y} \right|_{Y=f^+(x)} = \left. \frac{\partial p_1^{(0)}}{\partial y} \right|_{y=0^+}, \quad p_2^{(0)}|_{Y=f^+(x)} = p_1^{(0)}|_{y=0^+}, \quad (19)$$

$$\left. \frac{\partial p_2^{(0)}}{\partial Y} \right|_{Y=f^-(x)} = \left. \frac{\partial p_1^{(0)}}{\partial y} \right|_{y=0^-}, \quad p_2^{(0)}|_{Y=f^-(x)} = p_1^{(0)}|_{y=0^-}. \quad (20)$$

Solving (18) gives

$$p_2^{(0)} = A(x)Y + B(x).$$

Applying boundary conditions (19a) and (20a) implies

$$A(x) = \left. \frac{\partial p_1^{(0)}}{\partial y} \right|_{y=0^+} = \left. \frac{\partial p_1^{(0)}}{\partial y} \right|_{y=0^-},$$

while (19b) and (20b) imply

$$A(x)(f^+(x) - f^-(x)) = p_1^{(0)}|_{y=0^+} - p_1^{(0)}|_{y=0^-}.$$

It follows that

$$\left[\frac{\partial p_1^{(0)}}{\partial y} \right]_{y=0^-}^{y=0^+} = 0, \quad [p_1^{(0)}]_{y=0^-}^{y=0^+} = \left. \frac{\partial p_1^{(0)}}{\partial y} \right|_{y=0} (f^+(x) - f^-(x)), \quad |x| < a. \quad (21)$$

Implications. Here we have considered a crack filled with a much less permeable material than its surrounds, $k_2 \ll k_1$. In the case where the crack is thin, $\varepsilon f^+ - \varepsilon f^- = o(1/\lambda) = o(k_2/k_1)$, it has no effect on the flow in the surrounding region at leading order. If, however, the crack thickness lies in the range $1 \gg \varepsilon f^+ - \varepsilon f^- \gg k_2/k_1$ then it imposes the condition

$$\left. \frac{\partial p_1^{(0)}}{\partial y} \right|_{y=0} = 0, \quad |x| < a \quad (22)$$

on the surrounding flow. In other words it is, to leading order, impermeable to the flow.

Case (ii) $\lambda \ll 1$

Here we consider the case where the fault/crack is filled with a much more permeable material than its surrounds $k_2 \gg k_1$ (*i.e.* $\lambda \ll 1$). In this case the canonical scaling is $\lambda = \varepsilon$ and the expansions of p_1 and p_2 proceed as follows:

$$p_1 = p_1^{(0)} + \dots \quad \text{and} \quad p_2 = p_2^{(0)} + \varepsilon^2 p_2^{(1)}.$$

The leading order problem for $p_2^{(0)}$ is thus

$$\begin{aligned} \frac{\partial^2 p_2^{(0)}}{\partial Y^2} &= 0, \\ \frac{\partial p_2^{(0)}}{\partial Y} \Big|_{Y=f^+(x)} &= 0, \quad p_2^{(0)}|_{Y=f^+(x)} = p_1^{(0)}|_{y=0^+}, \\ \frac{\partial p_2^{(0)}}{\partial Y} \Big|_{Y=f^-(x)} &= 0, \quad p_2^{(0)}|_{Y=f^-(x)} = p_1^{(0)}|_{y=0^-}, \end{aligned}$$

from which it follows that

$$p_2^{(0)} = B(x) \quad \text{where} \quad B(x) = p_1^{(0)}|_{y=0^-} = p_1^{(0)}|_{y=0^+}. \quad (23)$$

In order to find further conditions on $p_1^{(0)}$ it is necessary to proceed to a higher order in p_2 , where we find

$$\frac{\partial^2 p_2^{(1)}}{\partial Y^2} + B''(x) = 0, \quad (24)$$

$$\frac{\partial p_2^{(1)}}{\partial Y} + f^{+'} \frac{\partial p_2^{(0)}}{\partial x} \Big|_{Y=f^+} = \frac{\partial p_1^{(0)}}{\partial Y} \Big|_{y=0^+}, \quad (25)$$

$$\frac{\partial p_2^{(1)}}{\partial Y} + f^{-'} \frac{\partial p_2^{(0)}}{\partial x} \Big|_{Y=f^-} = \frac{\partial p_1^{(0)}}{\partial Y} \Big|_{y=0^-}. \quad (26)$$

Integrating (24) between $Y = f^-$ and $Y = f^+$ and applying the conditions (25) and (26) at these two points results in the solvability condition

$$\left[\frac{\partial p_1^{(0)}}{\partial y} \right]_{y=0^-}^{y=0^+} = -\frac{\partial}{\partial x} ((f^+ - f^-)B'(x)).$$

Noting that $B(x)$ is defined in terms of $p_1^{(0)}$ by (23) we can rewrite this solvability condition and (23) as

$$\left[p_1^{(0)} \right]_{y=0^-}^{y=0^+} = 0, \quad \left[\frac{\partial p_1^{(0)}}{\partial y} \right]_{y=0^-}^{y=0^+} = -\frac{\partial}{\partial x} \left((f^+ - f^-) \frac{\partial p_1^{(0)}}{\partial x} \Big|_{y=0} \right). \quad (27)$$

Implications. Here we have considered a crack filled with a material which is much more permeable than its surrounds, $k_2 \gg k_1$. In the case where the crack is thin, $\varepsilon f^+ - \varepsilon f^- = o(\lambda) = o(k_1/k_2)$, it has no effect on the flow in the surrounding region at leading order. If, however, the crack thickness lies in the range $1 \gg \varepsilon f^+ - \varepsilon f^- \gg k_1/k_2$ then

$$\frac{\partial}{\partial x} p_1^{(0)}|_{y=0} = \frac{\text{const.}}{(f^+ - f^-)}, \quad |x| < a.$$

It follows, since $(f^+(a) - f^-(a)) = (f^+(-a) - f^-(-a)) = 0$, that the constant is zero, and the condition imposed on the surrounding flow by the crack/fault is

$$p_1^{(0)}|_{y=0} = 0. \quad (28)$$

Thus, the fault acts a channel along which flow may propagate with negligible pressure drop.

5.2 Darcy flow around linear faults

Motivated by the above observations, we now consider the idealised flow problem in which an array of two-dimensional slender faults within an otherwise homogeneous porous medium (of constant permeability k , which we now take to be 1 without loss of generality) may be modelled by an array of straight lines, of arbitrary lengths and orientations, on which either

$$\frac{\partial p}{\partial n} = 0 \quad (\text{an impermeable fault}),$$

or

$$p = 0 \quad (\text{an infinitely permeable fault}).$$

An oncoming uniform flow at infinity is assumed (though other far-field conditions could easily be dealt with). The general picture is illustrated in figure 2. Away from the faults the fluid velocity is given by the gradient of the pressure,

$$\mathbf{u} = -\nabla p,$$

where by incompressibility $\nabla^2 p = 0$.

Consider first a single fault in an oncoming uniform flow. Since the flow is two-dimensional, and the pressure is harmonic, we may define a complex potential for the flow by

$$w(z) = -p + i\psi,$$

where $z = x + iy$, and $\psi(x, y)$ is a streamfunction for the (steady) flow. The complex-conjugate velocity, $u - iv$, is then given by the derivative of the complex potential, dw/dz . For the cases under consideration we may write down the complex potential

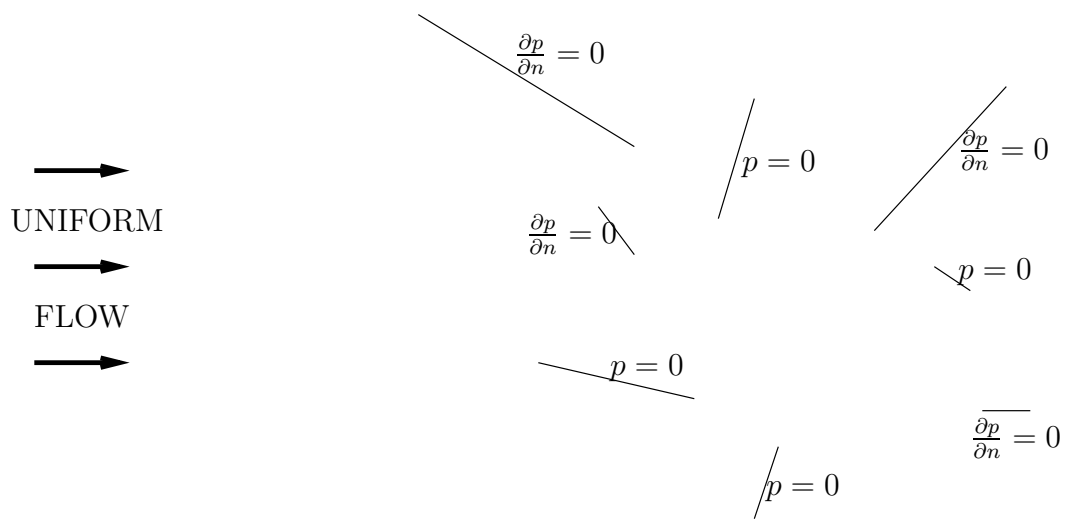


Figure 2: Schematic showing an array of arbitrary idealised faults in an oncoming uniform flow

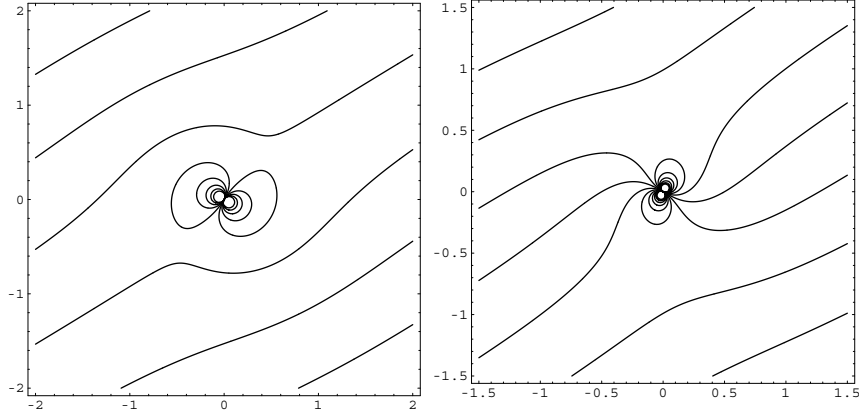


Figure 3: Streamline plots for the dipole singularity represented by a single fault in the far-field, (a) in the case $k = 0$, (b) in the case $k = \infty$. In both cases $U = 1$, $a = 1$, $\alpha = \pi/6$, $\beta = -\pi/6$.

(see, for example, Milne-Thomson, 1996) for the $k = 0$ case, and the $k = \infty$ case is readily obtained from this impermeable flat plate solution:

$$k = 0 : \quad w_0(z) = Ue^{-i\beta} \left(z \cos(\alpha - \beta) - i \sin(\alpha - \beta) \sqrt{z^2 - a^2 e^{2i\beta}} \right), \quad (29)$$

$$k = \infty : \quad w_\infty(z) = Ue^{-i\beta} \left(-iz \sin(\alpha - \beta) + \cos(\alpha - \beta) \sqrt{z^2 - a^2 e^{2i\beta}} \right), \quad (30)$$

where U is the flow speed at infinity, α is the angle this oncoming flow makes with the positive x -axis, β is the angle the fault makes with the x -axis, and $2a$ is the length of the fault (which is centred on $z = 0$). Far away from the fault we may expand these complex potentials in inverse powers of z , and we find that when viewed from afar, the faults look like dipole singularities in the flow field. Specifically, we find that for large $|z|$,

$$w_0(z) \sim Uze^{-i\alpha} + iUe^{i\beta} \frac{a^2 \sin(\alpha - \beta)}{2z} + \dots, \quad (31)$$

$$w_\infty(z) \sim Uze^{-i\alpha} - Ue^{i\beta} \frac{a^2 \cos(\alpha - \beta)}{2z} + \dots. \quad (32)$$

Streamlines for these singularities are given in figure 3.

When more than one fault is present, we would like to include extra dipole terms in (31) or (32), located at points z_{0j} , $z_{\infty j}$, with associated sizes a_{0j} , $a_{\infty j}$ and angles β_{0j} , $\beta_{\infty j}$, to be specified (the subscripts $0j$, ∞j refer to the j th singularity of type $k = 0$, ∞ , respectively). In general we cannot just add in such terms naively, as the dipoles will interact with one another, thus affecting the free-stream flow $Ue^{i\alpha}$ experienced by each dipole. Thus in general there will be extra undetermined parameters U_{0j} , $U_{\infty j}$ and α_{0j} , $\alpha_{\infty j}$ associated with each dipole. However, if the far-field flow is sufficiently strong that it dominates any dipole-dipole interactions we can take U and α to be fixed as a first

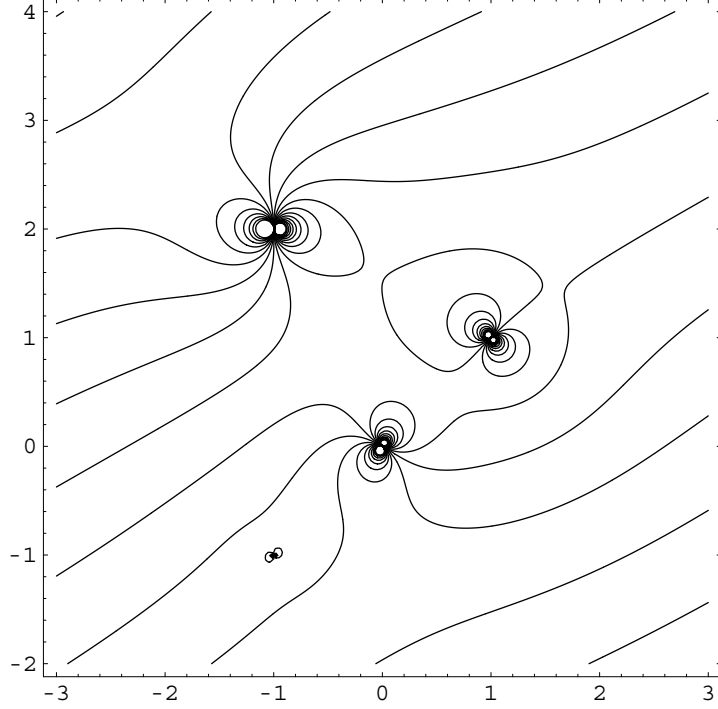


Figure 4: Streamline plots for two ‘ $k = 0$ ’ dipole singularities with parameters $z_{01} = 1 + i$, $z_{02} = -1 - i$, $a_{01} = 1$, $a_{02} = 3/4$, $\beta_{01} = -\pi/4$, $\beta_{02} = \pi/8$; and three ‘ $k = \infty$ ’ dipole singularities with parameters $z_{\infty 1} = 0$, $z_{\infty 2} = -1 + 2i$, $z_{\infty 3} = 2 - i$, $a_{\infty 1} = 3/2$, $a_{\infty 2} = 2$, $a_{\infty 3} = 3/4$, $\beta_{\infty 1} = -\pi/6$, $\beta_{\infty 2} = \pi/2$, $\beta_{\infty 3} = -\pi/3$. The (dominant) free-stream flow is given by $u + iv = e^{i\pi/6}$.

approximation, writing

$$w(z) = Uze^{-i\alpha} + \frac{iU}{2} \sum_{j=1}^{N_0} e^{i\beta_{0j}} \frac{a_{0j}^2 \sin(\alpha - \beta_{0j})}{z - z_{0j}} - \frac{U}{2} \sum_{j=1}^{N_\infty} e^{i\beta_{\infty j}} \frac{a_{\infty j}^2 \cos(\alpha - \beta_{\infty j})}{z - z_{\infty j}}.$$

Example streamlines for a flow of this kind are given in figure 4, which models five faults in an oncoming flow $u + iv = e^{i\pi/6}$.

There are two of type $k = 0$, with $z_{01} = 1 + i$, $z_{02} = -1 - i$, $a_{01} = 1$, $a_{02} = 3/4$, $\beta_{01} = -\pi/4$, $\beta_{02} = \pi/8$; and three of type $k = \infty$, with parameters $z_{\infty 1} = 0$, $z_{\infty 2} = -1 + 2i$, $z_{\infty 3} = 2 - i$, $a_{\infty 1} = 3/2$, $a_{\infty 2} = 2$, $a_{\infty 3} = 3/4$, $\beta_{\infty 1} = -\pi/6$, $\beta_{\infty 2} = \pi/2$, $\beta_{\infty 3} = -\pi/3$. Note that the $z_{\infty 3}$ singularity, being orientated perpendicular to the flow, has no effect on the streamlines. The equivalent situation for a $k = 0$ singularity would be when it is oriented parallel to the oncoming flow, which would then pass by unaffected.

In general, accounting for dipole-dipole interactions, the total streamfunction for an oncoming flow parallel to the x -axis, containing an arbitrary distribution of dipole

singularities, will be given by

$$w(z) = Uz + \sum_{j=1}^{N_0} w_{0j}(z) + \sum_{j=1}^{N_\infty} w_{\infty j}(z), \quad (33)$$

where

$$w_{0j}(z) = iU_{0j}e^{i\beta_{0j}} \frac{a_{0j}^2 \sin(\alpha_{0j} - \beta_{0j})}{2(z - z_{0j})} \quad (34)$$

$$w_{\infty j}(z) = -U_{\infty j}e^{i\beta_{\infty j}} \frac{a_{\infty j}^2 \cos(\alpha_{\infty j} - \beta_{\infty j})}{2(z - z_{\infty j})}. \quad (35)$$

The parameters U , β_{0j} , $\beta_{\infty j}$, a_{0j} , $a_{\infty j}$, z_{0j} , $z_{\infty j}$, are specified (the oncoming far-field flow speed; the inclinations of the faults to the x -axis; the sizes of the faults; and their locations), but the U_{0j} , $U_{\infty j}$, α_{0j} , $\alpha_{\infty j}$ are to be determined by requiring that the uniform oncoming streams $U_{0j} \exp(i\alpha_{0j})$, $U_{\infty j} \exp(i\alpha_{\infty j})$ experienced by each dipole are due to the combination of the far-field flow plus the flow generated by the other dipoles (but not itself), evaluated at the location of the dipole in question. Thus, these local ‘uniform streams’ must satisfy

$$U_{0j}e^{-i\alpha_{0j}} = \left. \frac{d}{dz} (w(z) - w_{0j}(z)) \right|_{z=z_{0j}}, \quad (36)$$

$$U_{\infty j}e^{-i\alpha_{\infty j}} = \left. \frac{d}{dz} (w(z) - w_{\infty j}(z)) \right|_{z=z_{\infty j}}, \quad (37)$$

giving $N_0 + N_\infty$ complex equations for the $2(N_0 + N_\infty)$ real unknowns U_{0j} , $U_{\infty j}$, α_{0j} , $\alpha_{\infty j}$.

An example of the streamlines when this dipole-dipole interaction is taken into account is given in figure 5. Figure 6 gives the corresponding streamlines when the interaction is neglected.

Summary: We can model an arbitrary array of interacting linear faults as a system of dipole singularities (of specified positions, strengths and orientations) in an oncoming (two-dimensional) far-field flow. Equations (33)–(37) give the closed system of equations required for the complex potential of the desired flow.

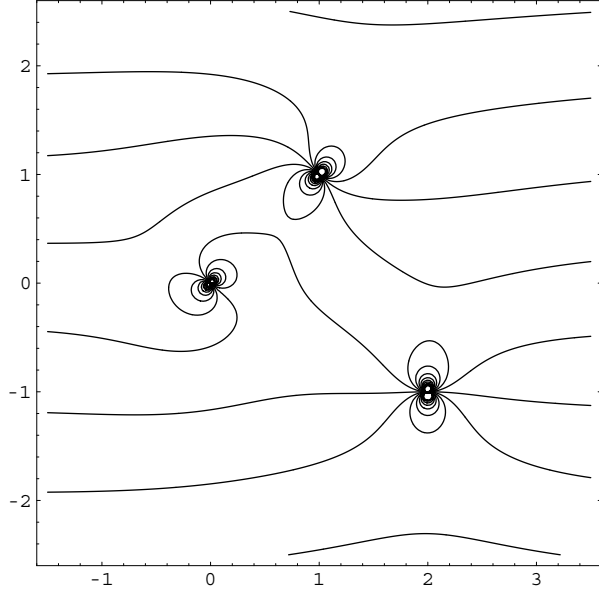


Figure 5: Streamline plots for interacting dipoles: one ‘ $k = 0$ ’ dipole singularity with parameters $z_{01} = 0$, $a_{01} = 1$, $\beta_{01} = \pi/4$; and two ‘ $k = \infty$ ’ dipole singularities with parameters $z_{\infty 1} = 1 + i$, $z_{\infty 2} = 2 - i$, $a_{\infty 1} = 1$, $a_{\infty 2} = 1$, $\beta_{\infty 1} = -\pi/4$, $\beta_{\infty 2} = 0$. The free-stream flow is given by $u + iv = 1$ ($U = 1$). Solving equations (36)–(37) yields $\alpha_{01} = 0.0848435$, $\alpha_{\infty 1} = -0.170154$, $\alpha_{\infty 2} = -0.0810698$, and $U_{01} = 0.907291$, $U_{\infty 1} = 1.06146$, $U_{\infty 2} = 0.957504$ (all α ’s would be zero and all U ’s equal to 1 if the interaction were neglected).

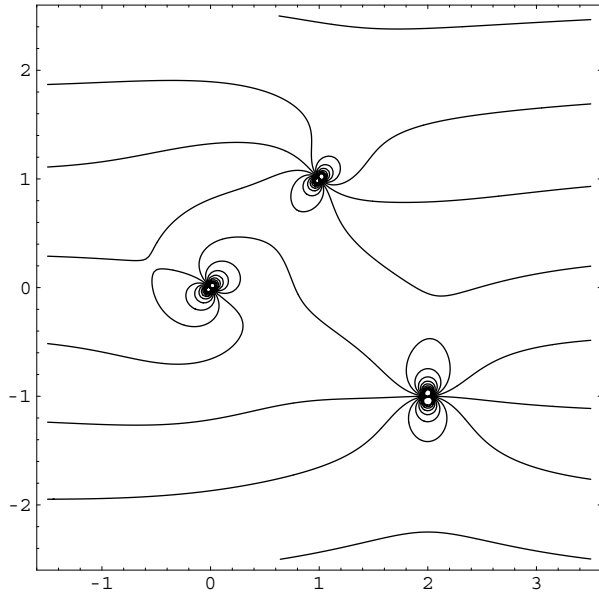


Figure 6: As for figure 5, but with the dipole interaction neglected. Thus in (33)–(35), the parameters are $z_{01} = 0$, $a_{01} = 1$, $\beta_{01} = \pi/4$, and $z_{\infty 1} = 1 + i$, $z_{\infty 2} = 2 - i$, $a_{\infty 1} = 1$, $a_{\infty 2} = 1$, $\beta_{\infty 1} = -\pi/4$, $\beta_{\infty 2} = 0$, and $\alpha_{ij} = 0$, $U_{ij} = 1$ for $i = 0, \infty$.

6 Boundary Element Methods

This section considers the solution of the flow problem by the Boundary Element Method (BEM).

6.1 Outline of the problem

The two-dimensional flow in a porous medium is governed by Darcy's law

$$\mathbf{v} = -k\nabla p$$

where p is the pressure and k is the permeability. The flow is conservative and so

$$\nabla \cdot \mathbf{v} = 0.$$

Combining these equations gives

$$\nabla(-k\nabla p) = 0. \quad (38)$$

Consider a canonical problem where equation (38) is solved in a rectangular region containing one or more obstacles that have either zero or infinite permeability. With the exception of the obstacles, the permeability in the flow region is assumed to be constant. The flow is driven by a pressure difference from left to right. The top and bottom boundaries are assumed to be impermeable and hence there is no normal flow. Similarly on the boundary of the separate obstacles with zero permeability there is no normal flow. On the boundary of an obstacle with infinite permeability the pressure is constant. The value of this constant is determined by the subsidiary condition

$$\oint_C k \frac{\partial p}{\partial n} ds = 0$$

where C is the boundary of the obstacle.

Define the flow region R to be the rectangle $(0, L) \times (0, H)$ excluding the obstacles. Let there be N_B obstacles having zero permeability with boundaries B_k , $k = 1, \dots, N_B$, and let there be N_C obstacles having infinite permeability with boundaries C_k , $k = 1, \dots, N_C$. It is assumed that none of the obstacles intersect. Then

$$\nabla^2 p = 0 \quad \text{in } R \quad (39)$$

with the boundary conditions

$$p(0, y) = p_0, \quad p(L, y) = 0, \quad \frac{\partial p(x, 0)}{\partial n} = 0, \quad \frac{\partial p(x, H)}{\partial n} = 0; \quad (40)$$

$$\frac{\partial p}{\partial n} = 0 \quad \text{on } B_k, \quad k = 1, \dots, N_B; \quad (41)$$

$$p = \text{constant on } C_k, \quad \oint_{C_k} \frac{\partial p}{\partial n} ds = 0, \quad k = 1, \dots, N_C. \quad (42)$$

6.2 Boundary element solution

Equations (39)–(42) will be solved numerically using the direct form of the boundary element method (BEM). Let δR denote the complete boundary of the region R , *i.e.* the boundary of the rectangle and each of the obstacles. From Green's theorem, equation (39) can be rewritten as

$$\frac{\alpha}{2\pi}p(\mathbf{a}) = \oint_{\delta R} \left(p(\mathbf{r}) \frac{\partial G}{\partial n}(\mathbf{r}; \mathbf{a}) - G(\mathbf{r}; \mathbf{a}) \frac{\partial p}{\partial n}(\mathbf{r}) \right) ds, \quad (43)$$

where $G(\mathbf{r}; \mathbf{a}) = \frac{1}{2\pi} \ln |\mathbf{r} - \mathbf{a}|$, \mathbf{a} is some fixed point on δR , and α is the internal angle between the two tangents to the boundary at \mathbf{a} . If the slope of δR is continuous then $\alpha = \pi$.

To calculate an approximate solution to this integral equation, the boundary δR is divided into small segments (elements). The functions p and $(\partial p/\partial n)$ are both approximated by piecewise polynomial functions of arc length s using nodal values on the elements.

Let the nodes be \mathbf{r}_i , $i = 1, \dots, M$ and let the variables p and $(\partial p/\partial n)$ have nodal values p_i and u_i respectively. Writing the piecewise polynomial basis functions as $\{\phi_i(s)\}$ then

$$p \simeq \sum_{j=1}^M p_j \phi_j(s) \quad \text{and} \quad \frac{\partial p}{\partial n} \simeq \sum_{j=1}^M u_j \phi_j(s). \quad (44)$$

Equation (43) is valid for any point \mathbf{a} on δR and so applying it to the nodes $\{\mathbf{r}_i\}$ in turn and substituting the approximations for p and $(\partial p/\partial n)$ defined by equations (44) gives

$$\frac{\alpha_i}{2\pi}p_i = \oint_{\delta R} \left(\sum_{j=1}^M p_j \phi_j(s) \frac{\partial G}{\partial n}(\mathbf{r}; \mathbf{r}_i) - G(\mathbf{r}; \mathbf{r}_i) \sum_{j=1}^M u_j \phi_j(s) \right) ds, \quad i = 1, \dots, M,$$

where α_i is the internal angle between the two tangents to the boundary at \mathbf{r}_i .

Reversing the order of integration and summation then gives the linear algebraic system

$$\mathbf{H}\mathbf{p} = \mathbf{G}\mathbf{u}, \quad (45)$$

where

$$G_{i,j} = \oint_{\delta R} \phi_j(s) G(\mathbf{r}; \mathbf{r}_i) ds \quad \text{and} \quad H_{i,j} = \oint_{\delta R} \phi_j(s) \frac{\partial G}{\partial n}(\mathbf{r}; \mathbf{r}_i) ds - \frac{\alpha_i}{2\pi} \delta_{i,j}$$

and the vectors of unknowns are the nodal values of p and $(\partial p/\partial n)$, $\mathbf{p} = (p_1, \dots, p_M)$ and $\mathbf{u} = (u_1, \dots, u_M)$.

Equation (45) provides M equations in $2M$ unknowns. From the boundary conditions (40), the value of p_i or u_i is known at each node on the boundary of the rectangle and can

be substituted directly into (45). Similarly, from the boundary conditions (41), the value of u_i is known at each node on the boundary, B_k , of the obstacles with zero permeability and can also be substituted directly into (45).

The situation on the boundary of the obstacles with infinite permeability is different since neither unknown is given explicitly. Let S_k be the set of nodes on the boundary C_k and introduce additional variables $p_{M+1}, p_{M+2}, \dots, p_{M+N_C}$. Then the first of boundary conditions (42) becomes

$$p_i = p_{M+k} \quad i \in S_k$$

and p_{M+k} is substituted for each p_i on C_k into equation (45).

Applying the approximations for $(\partial p / \partial n)$ defined by (44) to the second of the boundary conditions (42) gives the additional equations

$$\sum_{j \in S_k} B_j u_j = 0, \quad k = 1, \dots, N_C, \quad \text{where } B_j = \oint_{\delta R} \phi_j(s) ds. \quad (46)$$

Equations (45) and (46) can now be rearranged as a set of $(M + N_C)$ linear equations for one unknown at each of the M nodes and the N_C additional pressure variables.

6.3 Comparison of methods

The solution by BEM is computationally much cheaper than a full CFD computation, but the limitation of a BEM solution is that the values of p and $(\partial p / \partial n)$ are only computed on the boundaries of the flow region (including the obstacles). However it provides key information to allow experiments with a range of obstacles. In particular the normal velocity at the outlet ($= k(\partial p / \partial n)$) is computed and this can be trivially integrated (numerically) to give the total outlet flux. The normal velocity around each of the obstacles with infinite permeability is also computed and so the effect of such an obstacle on the flow can be seen. Similarly the pressure around each of the obstacles with zero permeability is computed.

The solution by BEM allows greater flexibility than an analytic solution (*e.g.* complex variable). In particular there can be any number of obstacles of arbitrary shape in the flow, and the flow region can have arbitrary boundaries.

6.4 Results

The following results are intended to be illustrative of numerical experiments that could be conducted. All computations were performed using a rectangle of length $L = 3$ and width $H = 2$. The permeability was taken to $k = 1$ and a pressure difference of $p_0 = 3$ was imposed. Hence the undisturbed flow has a uniform velocity of $U = 1$ in the x -direction and the total flux through the outlet at $x = 3$ is 2.

A single obstacle in the form of a thin rectangle representing a slit was introduced with its centre at the centre of the flow region. The slit had length $a = 1$ and width $w = 0.05$. The slit was placed at an angle β to the x -axis and the cases of a zero or infinite permeability slit were considered separately.

The computations were all performed using the simplest elements — piecewise constant approximations on straight line elements.

Slit with zero permeability

If a slit with zero permeability having zero width were placed parallel to the x -axis ($\beta = 0$) it would have no effect on the flow. However using a small width of $w = 0.05$ produces a small decrease in total outlet flux. A series of experiments were conducted using various values of β and the results are summarized in figure 7. As the angle of incidence is increased the outlet flux decreases further, as shown by the solid line in figure 7. When $\beta = \pi/2$, the effect is greatest with the slit perpendicular to the flow and blocking half the width of the channel.

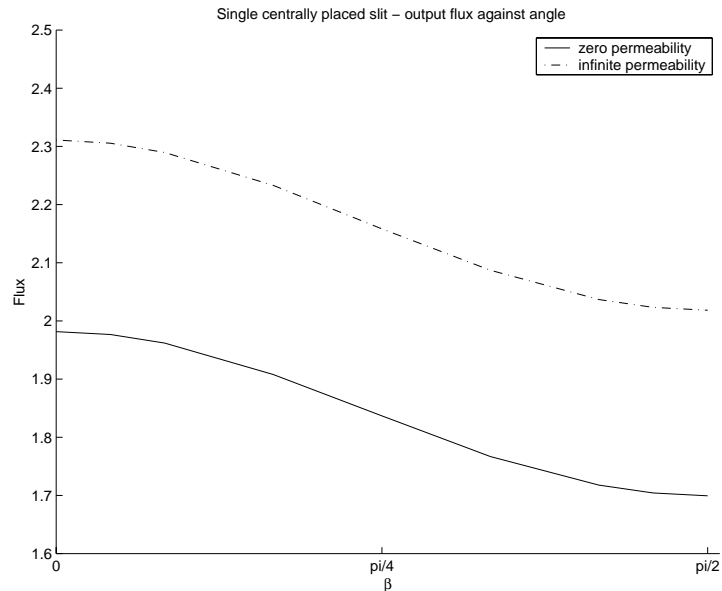


Figure 7: Single obstacle: outlet flux against angle of incidence.

Slit with infinite permeability

If a slit with infinite permeability having zero width were placed perpendicular to the x -axis ($\beta = \pi/2$) it would also have no effect on the flow. However using a small width of $w = 0.05$ produces a small increase in total outlet flux. As the angle of incidence is decreased the outlet flux increases further, as shown by the dotted line in figure 7. When $\beta = 0$, the effect is greatest, with the slit parallel to the flow and providing a ‘shortcut’.

A graph of the normal velocity around the slit (plotted against arc length) for the case $\beta = \pi/4$ is shown in figure 8. A positive value indicates flow into the main flow region,

and a negative value indicates flow into the slit. The total flux through the slit in this case is 1.1197, which is approximately half of the outlet flux of 2.1588. The slit only extends for 35% of the width of the channel and so the attraction of the infinite permeability slit is seen.

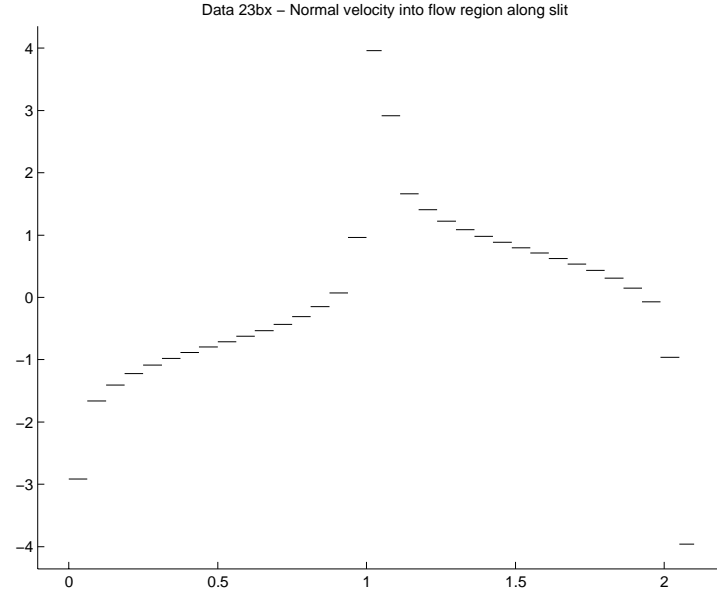


Figure 8: Computed normal velocity along slit of infinite permeability ($\beta = \pi/4$).

Comparison with complex variable solution

The BEM results were validated by comparison with the complex variable solution of flow past a slit of zero width in an infinite flow field (see section 5). The results for both the zero permeability and infinite permeability slits agreed well qualitatively. Note that since the flow field conditions are different we would not expect very close agreement.

For the particular case of a slit with infinite permeability, the complex variable solution gives the normal velocity along the slit as

$$u_n = U \left(\frac{r}{\sqrt{a^2 - r^2}} \cos \beta \pm \sin \beta \right). \quad (47)$$

Figure 9 shows a graph of the normal velocity calculated from equation (47) for the particular case $\beta = \pi/4$. The similarity between figures 8 and 9 is easily seen.

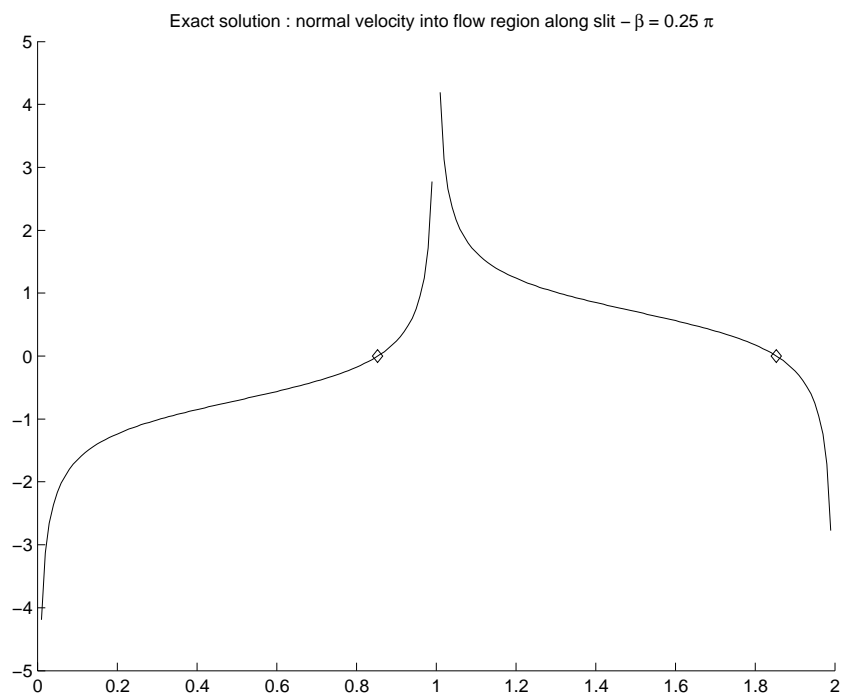


Figure 9: Normal velocity along slit of infinite permeability (exact solution, $\beta = \pi/4$).

References

- Bartlett, M.: 1978, *An Introduction to Stochastic Processes*. Cambridge UK: Cambridge University Press, 3rd edition.
- Craig, P., M. Goldstein, J. Rougier, and A. Seheult: 2001, 'Bayesian Forecasting for Complex Systems Using Computer Simulators'. *Journal of the American Statistical Association* **96**, 717–729.
- Craig, P., M. Goldstein, A. Seheult, and J. Smith: 1996, 'Bayes Linear Strategies for Matching Hydrocarbon Reservoir History'. In: J. Bernardo, J. Berger, A. Dawid, and A. Smith (eds.): *Bayesian Statistics 5*. Oxford: Clarendon Press, pp. 69–95.
- Craig, P., M. Goldstein, A. Seheult, and J. Smith: 1997, 'Pressure Matching for Hydrocarbon Reservoirs: A Case Study in the Use of Bayes Linear Strategies for Large Computer Experiments'. In: C. Gatsonis, J. Hodges, R. Kass, R. McCulloch, P. Rossi, and N. Singpurwalla (eds.): *Case Studies in Bayesian Statistics III*. New York: Springer-Verlag, pp. 37–87. With discussion.
- Craig, P., M. Goldstein, A. Seheult, and J. Smith: 1998, 'Constructing Partial Prior Specifications for Models of Complex Physical Systems'. *The Statistician* **47**, 37–53. With discussion.
- Evans, M. and T. Swartz: 2000, *Approximating Integrals via Monte Carlo and Deterministic Methods*. Oxford: Oxford University Press.
- Goldstein, M.: 1999, 'Bayes Linear Analysis'. In: *Encyclopaedia of Statistical Sciences, update vol. 3*. London: John Wiley & Sons, pp. 29–34.
- Goldstein, M. and J. Rougier: 2004, 'Probabilistic Formulations for Transferring Inferences from Mathematical Models to Physical Systems'. *SIAM Journal on Scientific Computing*. In press.
- Handcock, M. and M. Stein: 1993, 'A Bayesian Analysis of Kriging'. *Technometrics* **35**, 403–410.
- Kennedy, M. and A. O'Hagan: 2001, 'Bayesian calibration of computer models'. *Journal of the Royal Statistical Society, Series B* **63**, 425–464. With discussion.
- Milne-Thomson, L.: 1996, *Theoretical Hydrodynamics*. Dover.
- Ripley, B.: 1987, *Stochastic Simulation*. New York: John Wiley & Sons.
- Robert, C. and G. Casella: 1999, *Monte Carlo Statistical Methods*. New York: Springer.
- Smith, A. and A. Gelfand: 1992, 'Bayesian Statistics Without Tears: A Sampling-Resampling Perspective'. *The American Statistician* **46**, 84–88.